

Dual-wavelength ultraviolet photodetector based on vertical (Al,Ga)N nanowires and graphene

Min Zhou(周敏), Yukun Zhao(赵宇坤), Lifeng Bian(边历峰), Jianya Zhang(张建亚), Wenxian Yang(杨文献), Yuanyuan Wu(吴渊渊), Zhiwei Xing(邢志伟), Min Jiang(蒋敏), and Shulong Lu(陆书龙)

Citation: Chin. Phys. B, 2021, 30 (**7**): 078506. DOI: 10.1088/1674-1056/abff23
Journal homepage: http://cpb.iphy.ac.cn; http://iopscience.iop.org/cpb

What follows is a list of articles you may be interested in

Effect of electrical contact on performance of WSe_2 field effect transistors

Yi-Di Pang(庞奕荻), En-Xiu Wu(武恩秀), Zhi-Hao Xu(徐志昊), Xiao-Dong Hu(胡晓东), Sen Wu(吴森), Lin-Yan Xu(徐临燕), and Jing Liu(刘晶)

Chin. Phys. B, 2021, 30 (**6**): 068501. DOI: 10.1088/1674-1056/abd752

Graphene/$SrTiO_3$ interface-based UV photodetectors with high responsivity

Heng Yue(岳恒), Anqi Hu(胡安琪), Qiaoli Liu(刘巧莉), Huijun Tian(田慧军), Chengri Hu(胡成日), Xiansong Ren(任显松), Nianyu Chen(陈年域), Chen Ge(葛琛), Kuijuan Jin(金奎娟), and Xia Guo(郭霞)

Chin. Phys. B, 2021, 30 (**3**): 038502. DOI: 10.1088/1674-1056/abda2e

A method to extend wavelength into middle-wavelength infrared based on InAsSb/(Al)GaSb interband transition quantum well infrared photodetector

Xuan-Zhang Li(李炫璋), Ling Sun(孙令), Jin-Lei Lu(鲁金蕾), Jie Liu(刘洁), Chen Yue(岳琛), Li-Li Xie(谢莉莉), Wen-Xin Wang(王文新), Hong Chen(陈弘), Hai-Qiang Jia(贾海强), Lu Wang(王禄)

Chin. Phys. B, 2020, 29 (**3**): 038504. DOI: 10.1088/1674-1056/ab6969

Evaluation of current and temperature effects on optical performance of InGaAlP thin-film SMD LED mounted on different substrate packages

Muna E. Raypah, Mutharasu Devarajan, Fauziah Sulaiman

Chin. Phys. B, 2017, 26 (**7**): 078503. DOI: 10.1088/1674-1056/26/7/078503

White organic light-emitting diodes based on combined electromer and monomer emission in doubly-doped polymers

Meng Ling-Chuan, Lou Zhi-Dong, Yang Sheng-Yi, Hou Yan-Bing, Teng Feng, Liu Xiao-Jun, Li Yun-Bai

Chin. Phys. B, 2012, 21 (**8**): 088504. DOI: 10.1088/1674-1056/21/8/088504

Dual-wavelength ultraviolet photodetector based on vertical (Al,Ga)N nanowires and graphene*

Min Zhou(周敏)[1,2], Yukun Zhao(赵宇坤)[1,†], Lifeng Bian(边历峰)[1], Jianya Zhang(张建亚)[1,2], Wenxian Yang(杨文献)[1], Yuanyuan Wu(吴渊渊)[1], Zhiwei Xing(邢志伟)[1,2], Min Jiang(蒋敏)[1,2], and Shulong Lu(陆书龙)[1,‡]

[1] *Suzhou Institute of Nano-Tech and Nano-Bionics (SINANO), Chinese Academy of Sciences (CAS), Suzhou* 215123, *China*
[2] *School of Nano-Tech and Nano-Bionics, University of Science and Technology of China, Hefei* 230026, *China*

(Received 5 February 2021; revised manuscript received 9 April 2021; accepted manuscript online 8 May 2021)

Due to the wide application of UV-A (320 nm–400 nm) and UV-C (200 nm–280 nm) photodetectors, dual-wavelength (UV-A/UV-C) photodetectors are promising for future markets. A dual-wavelength UV photodetector based on vertical (Al,Ga)N nanowires and graphene has been demonstrated successfully, in which graphene is used as a transparent electrode. Both UV-A and UV-C responses can be clearly detected by the device, and the rejection ratio ($R_{254\ nm}/R_{450\ nm}$) exceeds 35 times at an applied bias of −2 V. The short response time of the device is less than 20 ms. Furthermore, the underlying mechanism of double ultraviolet responses has also been analyzed systematically. The dual-wavelength detections could mainly result from the appropriate ratio of the thicknesses and the enough energy band difference of (Al,Ga)N and GaN sections.

Keywords: dual-wavelength ultraviolet photodetector, (Al,Ga)N nanowire, graphene, molecular beam epitaxy

PACS: 85.60.Gz, 78.67.Uh, 78.66.Fd, 85.60.Bt **DOI:** 10.1088/1674-1056/abff23

1. Introduction

In recent years, due to a wide range of applications in communication, flame sensors, ozone monitoring, and even ultraviolet (UV) astronomy, people have great interest in UV-A (320 nm–400 nm) and UV-C (200 nm–280 nm) photodetectors.[1,2] By reducing false positive detection, dual-wavelength photodetectors are beneficial to increase accuracy.[3] In general, measuring dual-wavelength bands typically requires double detectors with separate cooling assemblies and readout circuits.[3,4] However, it could increase the manufacturing costs and enhance the difficulties of assembling double different detectors.[3,5] A single photodetector responding in dual wavelengths paves an efficient way to overcome the above problems.[3] For example, dual-wavelength detection can clearly distinguish the missile from its plume and can reduce mine detection errors.[3] Hence, dual-wavelength (UV-A/UV-C) photodetectors are necessary and promising for future markets of UV detections.

Due to the continuous adjustable bandgap covering the range from about 200 nm to 365 nm, (Al,Ga)N can shield the interference of visible light without any special filters compared with Si.[6–10] Thus, (Al,Ga)N is beneficial for detector miniaturization and saving the cost of filters. In addition to the extraordinary characteristics of being nontoxic, long lifetime and high stability against UV radiation, (Al,Ga)N is an ideal material for making UV photodetectors.[6–9,11] Moreover, compared with thin films or bulk, nanowires show better photoelectric properties due to its large specific surface area and smaller size.[12–14] Nanowires have special ability for selectively enhancing nanoscale light absorption due to their optical properties.[15] However, to date, most UV detectors are based on thin films or bulk materials, and few groups have studied UV detectors based on vertical (Al,Ga)N nanowires.[16,17] In our previous work, a UV detector based on (Al,Ga)N nanowires only achieved a single response in the UV range.[16] The results agree with those from another group.[17] The underlying mechanism is still unclear. Therefore, it is promising but highly challenging to achieve dual-wavelength UV photodetectors based on vertical (Al,Ga)N nanowires.

In this work, we demonstrate a dual-wavelength (UV-A/UV-C) detector based on (Al,Ga)N/GaN nanowires. The dual-wavelength detector provides double responses in UV-A and UV-C regions. The maximum responsivity of UV-C band is over 15.5 mA·W^{-1}, while that of UV-A band is over 5.0 mA·W^{-1}. Due to the good transparency and conductivity, graphene is utilized as a current collecting layer. The underlying mechanism contributing to the double responses has been studied systematically.

*Project supported by the National Key Research and Development Program of China (Grant No. 2018YFB0406602), Natural Science Foundation of Jiangsu Province, China (Grant No. BK20180252), Key Research Program of Frontier Sciences, CAS (Grant No. ZDBS-LY-JSC034), the National Natural Science Foundation of China (Grant Nos. 61804163, 61875224, and 61827823), the Key Research and Development Program of Jiangsu Province, China (Grant No. BE2018005), Natural Science Foundation of Jiangxi Province, China (Grant No. 20192BBEL50033), Research Program of Scientific Instrument, Equipment of CAS (Grant No. YJKYYQ20200073), SINANO (Grant Nos. Y8AAQ21001 and Y4JAQ21001), and Vacuum Interconnected Nanotech Workstation (Grant Nos. Nano-X and B2006).

†Corresponding author. E-mail: ykzhao2017@sinano.ac.cn
‡Corresponding author. E-mail: sllu2008@sinano.ac.cn

© 2021 Chinese Physical Society and IOP Publishing Ltd

2. Experiments

Vertical (Al,Ga)N nanowires were grown on Si substrate by molecular beam epitaxy (MBE). Prior to the MBE growth, the Si (111) substrate in the growth chamber should be heated up to about 900 °C for 15 min to eliminate the native oxides. The 7×7 reconstruction was normally observed after this treatment, indicative of a clean surface. Initially, an AlN buffer layer was grown with a nominal Al flux of ~ 3.0 nm·min^{-1} for 1.0 min. Subsequently, GaN nanowires were grown with a Ga flux of $\sim 3.0\times10^{-8}$ Torr for about 100 min with a growth rate of ~ 3.8 nm·min^{-1}. The substrate temperature is set to be 770 °C. The deposited GaN initially forms into islands which act as a material collector and a seed for the nanowires.[16] After the growth of GaN section, the (Al,Ga)N section was grown for 90 min with a constant substrate temperature of 770 °C. Two thin AlN sections were inset into the (Al,Ga)N section as mark layers. When start and finish growing the (Al,Ga)N segment, the shutters of Al and Ga cells were opened and closed simultaneously by the software. To increase the nanowire uniformity, samples were rotated with a rate of 120 °/s during the growth process.

To fabricate the photodetectors, a thick SiO_2 film was deposited on the surface of nanowires. Then some parts of the SiO_2 film were removed to form a square area to expose some nanowires. After that, Ti/Al (50/200 nm) was deposited as a backside electrode on the backside of the Si substrate by electron beam evaporation. Ohmic contact is formed by annealing at 400 °C in N_2 atmosphere for 30 min. Graphene was transferred to the top of the nanowires by wet transfer as a transparent current collecting layer.[18] The transfer process is shown in Fig. SI (supporting information). Finally, Ti/Pt/Au (25/55/300 nm) was deposited on the graphene surface as an electrode.

Scanning electron microscopy (SEM), scanning transmission electron microscopy (STEM) and high-resolution energy dispersive x-ray (EDX) mapping were used to characterize the surface morphology and element distribution of nanowires. The STEM samples were prepared by focused ion beam (FIB). The intrinsic emission spectra of (Al,Ga)N nanowires were measured by photoluminescence (PL). The current–voltage and transient responses characteristics of the (Al,Ga)N photodetectors were measured by the probe station. The spectral response measurement employed a self-constructed photoelectric measurement system mainly consisting of an optical chopper, a xenon lamp, a data processing center and a power supply.

3. Results and discussion

From the top-view and side-view SEM images in Fig. 1(a), the vertical nanowires are formed and distributed on the Si substrate with good verticality and small fluctuation. As shown in Fig. 1(b), vertical (Al,Ga)N sections have been fabricated as designed. The lateral surface of GaN segment is wrapped by (Al,Ga)N section, forming a core-shell structure. Fig. 1(c) illustrates element distribution from the top to bottom regions of a nanowire, which further demonstrates the existence of (Al,Ga)N section.

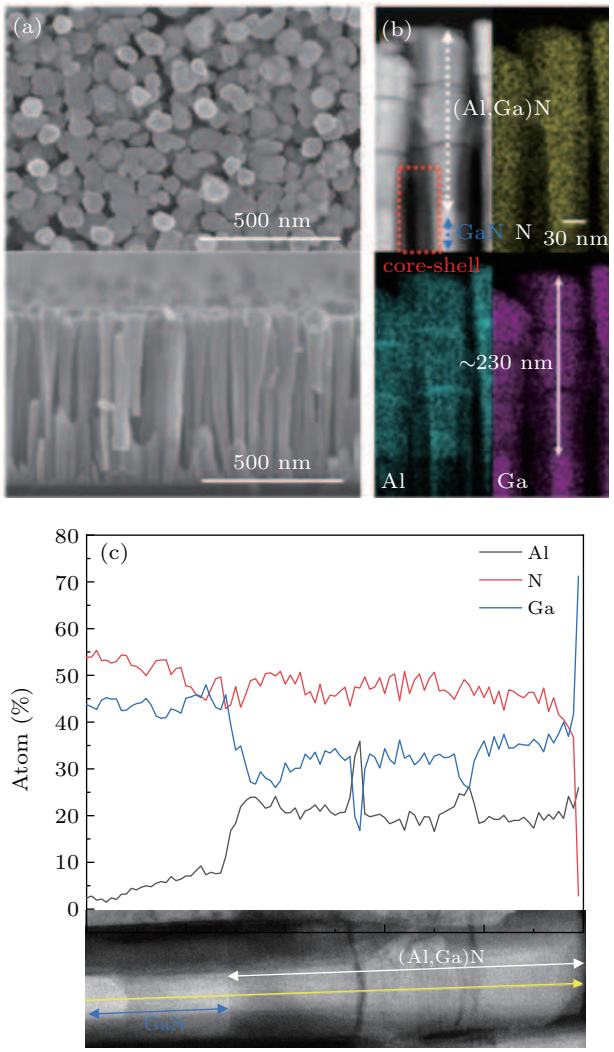


Fig. 1. (a) SEM images of vertical (Al,Ga)N nanowires. (b) High angle annular dark field STEM images of vertical (Al,Ga)N nanowires. (c) High-resolution EDX mapping analysis about the element distributions of vertical (Al,Ga)N nanowires.

The PL spectra of (Al, Ga)N nanowires are shown in Fig. 2(a). E_g(AlN) and E_g(GaN) are the bandgap of AlN and GaN at room temperature, which are 6.2 eV and 3.4 eV, respectively,[19,20]

$$E_g(\mathrm{Al}_x\mathrm{Ga}_{1-x}\mathrm{N}) = x\cdot E_g(\mathrm{AlN}) + (1-x)\cdot E_g(\mathrm{GaN}) - b\cdot x\cdot(1-x). \quad (1)$$

According to Eq. (1), the Al content is calculated to be about 18%.[21] As the Raman spectrum shown in Fig. 2(b), three obvious peaks exist, namely D peak, G peak and 2D peak. G peak (~ 1581 cm^{-1}) is caused by the in-plane vibration of sp^2 hybrid carbon atoms, which proves the existence of graphene

after fabricating detectors.[16] D peak ($\sim$ 1343 cm^{-1}) is related to graphene defects[22] and the 2D peak ($\sim$ 2693 cm^{-1}) in graphene is due to two phonons resonance.[23] The number of graphene layers is reflected by the ratio of 2D peak intensity to G peak intensity (I_{2D}/I_G). By calculating, the ratio I_{2D}/I_G is 0.56, indicating that graphene has a multilayer structure.[24,25] The I–V characteristics of the detector under dark, UV-A and UV-C illumination (at 254 nm and 365 nm, corresponding to AlGaN and GaN band edge, respectively) were measured by Agilent B1505A instrument for observing the rectification and photo response characteristics. As shown in Fig. 2(c), the I–V curves of the detector under no illumination are nonlinear, which indicates that Schottky contact exists between graphene and nanowires.[26] In addition, under 254 nm and 365 nm illumination, the asymmetry is more obvious relative to the bias direction, indicating that the detector has good response characteristics to UV-C and UV-A illumination. Furthermore, the dark current of the detector is 34.6 nA at -2 V with an area of 0.96 mm^2.

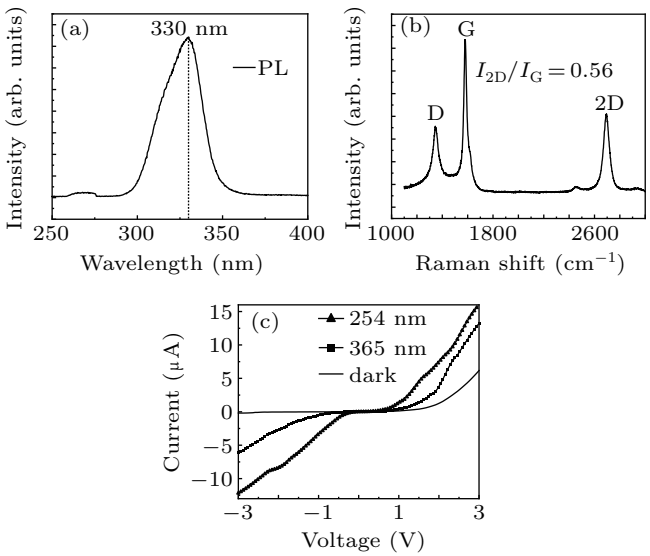


Fig. 2. (a) PL spectrum of vertical (Al, Ga)N nanowire array. (b) Raman spectrum of the graphene film measured with an excitation wavelength of 532 nm. (c) Current–voltage characteristics of detector in dark, UV-A and UV-C illumination measured at room temperature.

Figure 3(a) shows a schematic diagram of the detector under the measurement of responsiveness. When testing responsiveness, a bias of -2 V is applied to the detector. The spectral responsivity of the detector is defined as the photocurrent output under the action of the unit incident radiation power.[27] As shown in Fig. 3(b), the black triangle represents the experimental data, and the red line represents the data smoothed by 12 points. It is clearly illustrated that the detector shows a dual-wavelength response in the band of 240 nm–400 nm. The maximum responsivity of the first response in the range of UV-C band exceeds 15.5 mA·W^{-1}, while that of the second response in the range of UV-A band is over 5.0 mA·W^{-1}. The rejection ratio ($R_{254\ nm}/R_{450\ nm}$) exceeds 35 times at an applied bias of -2 V.

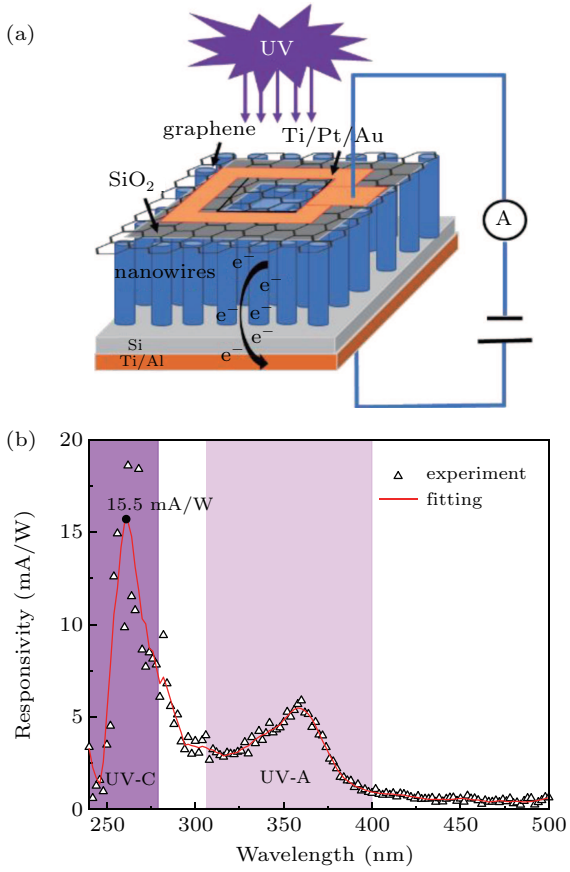


Fig. 3. (a) Schematic diagram of detector. (b) Spectral response of the detector at the bias at -2 V.

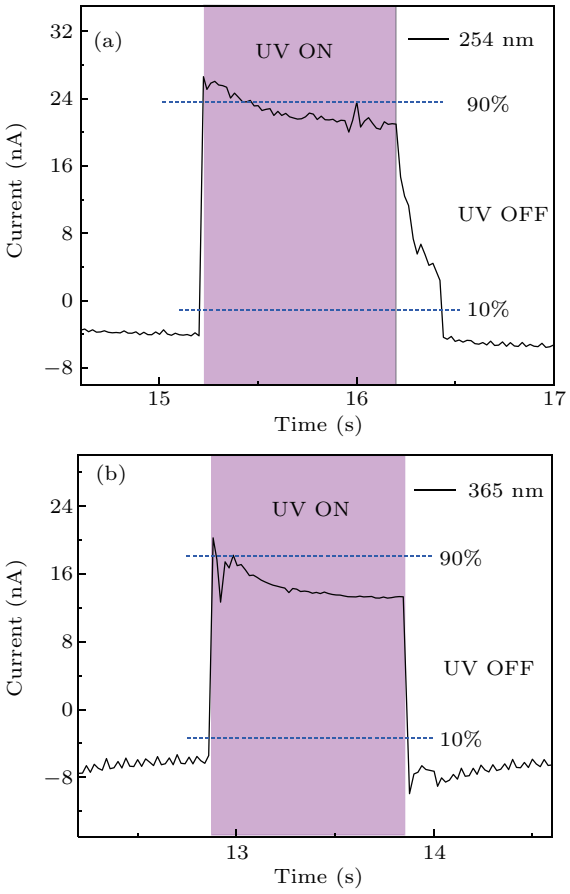


Fig. 4. (a) Transient response of the detector to 254 nm (UV-C) illumination. (b) Transient response of the detector to 365 nm (UV-A) illumination.

Figures 4(a) and 4(b) show the current switching characteristics of the detector under UV-C (254 nm) and UV-A (365 nm) illumination at −2 V, corresponding to the first and the second responses, respectively. The on/off current can increase/decrease in a certain period of time with/without UV irradiation. All measurements have been conducted at room temperature in air. The rise time (defined as the time when the current rises from 10% to 90% of the peak current value) is less than 20 ms and 20 ms and the decay time (defined as the time when the current drops from 90% to 10% of the peak current value) is less than 960 ms and 955 ms under 254 nm and 365 nm illumination, respectively. The accuracy of our equipment is 20 ms. By comparing the key parameters listed in Table 1, graphene/AlGaN /GaN nanowires has advantages in transient response compared with some recent new photodetectors.[28–33]

Table 1. Comparison of response time between this work and some state-of-the-art reports.

Materials	Wavelength (nm)	Rise time/decay time (ms)	Ref.
Ag NW/ZnO/Ag NW	365	1830/1750	[28]
Nanoporous GaN/β-Ga_2O_3	360	1090/790	[29]
ZnS/GaN	365	159/> 68.7	[30]
GaN nanotowers/Si(111)	325	1160/1010	[31]
Au NP/GaN	365	2900/6200	[32]
GaN/MoO_{3-x} nanorod array	355	$0.345/127 \times 10^{-6}$	[33]
Graphene/AlGaN/GaN nanowires	254	< 20/960	this work
Graphene/AlGaN/GaN nanowires	365	< 20/955	this work

In order to further study the underlying mechanism of dual-wavelength UV detector, we plot the schematic diagrams in Fig. 5. At −2 V bias voltage, when UV light irradiates on the photodetector (Fig. 5(a)), photons can reach the nanowires through the graphene as it is thin enough and transparent in the UV range. Then, photons can be absorbed by (Al,Ga)N and GaN sections, producing electron-hole pairs. Due to the core-shell structure of nanowires, there are two ways (Fig. 5(a) 1 and 2) for photogenerated carriers to diffuse to the electrodes. "1" in Fig. 5(a) indicates the common way, and carriers are diffused along the vertical direction to both sides of the nanowires. The other way ("2" in Fig. 5(a)) is utilized for carriers to diffuse along shell walls, which paves an addition way for the carrier transports. Therefore, electrons are easier to be collected, contributing to the fast response speed (Table 1). Figure 5(b) shows the schematic of energy band of (Al,Ga)N nanowires in this work, while Figs. 5(c) and 5(d) are corresponding to the (Al,Ga)N nanowires from Refs. [17] and [16], respectively. As illustrated in Fig. 5(b), due to AlN sections are very thin, it is easy for the photogenerated carriers to pass through by diffusion or tunneling. Therefore, the photogenerated electrons within the (Al,Ga)N section can also pass through the GaN layer and be collected by the electrode.

Although the (Al,Ga)N nanowires from Ref. [17] has GaN section, the responsivity does not have an obvious peak corresponding to GaN (Fig. 5(c) from Ref. [17]). It is proposed that the main reason is the ratio of the thicknesses of (Al,Ga)N and GaN sections as shown below:

$$\eta = \frac{T_{(\mathrm{Al,Ga})\mathrm{N}}}{T_{\mathrm{GaN}}}, \tag{2}$$

$$\Delta E_{\mathrm{g}} = E_{\mathrm{g}}((\mathrm{Al,Ga})\mathrm{N}) - E_{\mathrm{g}}(\mathrm{GaN}). \tag{3}$$

Here T is defined as the thickness. The η in Ref. [17] is equal to 3, which is much larger than that η (~ 0.61) in this work. Thus, compared to that in Fig. 5(b), the smaller proportion of holes generated within the GaN section (Fig. 5(c)) can cross the (Al,Ga)N layer and then be collected by the electrode. In addition, although the η (~ 0.29) in Ref. [16] is smaller than that in this work, we still cannot achieve the obvious dual-wavelength responses (Fig. 5(d) from Ref. [16]). According to the PL spectra in Fig. 2(a) and Ref. [16], as well as Eqs. (1) and (3), the composition of Al in Ref. [16] is calculated to be about 6.5%, which is much smaller than that ($\sim$ 18%) in this work. When the Al composition is very low, the band gap of (Al,Ga)N section is pretty close to GaN. In other words, when the difference (ΔE_{g}) of the energy bands of (Al,Ga)N and GaN sections is very small, it should be difficult to separate the responses of (Al,Ga)N and GaN sections to achieve dual-wavelength responses. As a result, both η and ΔE_{g} are the key parameters to achieve dual-wavelength UV responses.

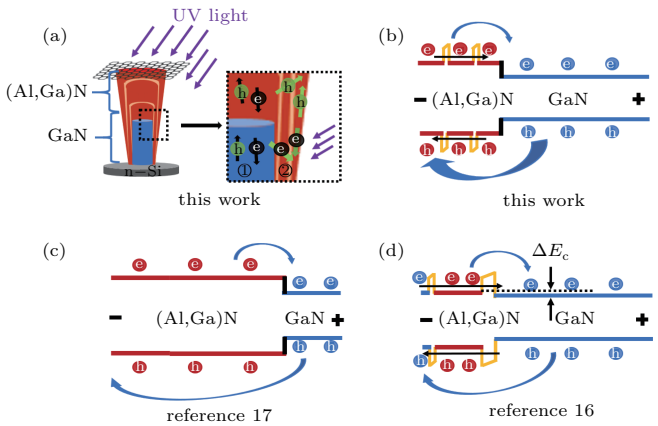


Fig. 5. (a) Schematic diagram of UV irradiation on the photodetector. Enlarged image indicates the diffusion of photogenerated carriers within the core-shell structure. (b) Energy band diagram of the (Al,Ga)N nanowires under UV illumination in this work. (c) Energy band diagram of the (Al,Ga)N nanowires from Ref. [17]. (d) Energy band diagram of the (Al,Ga)N nanowires from Ref. [16].

4. Conclusion

In summary, we demonstrate a dual-wavelength (UV-A/UV-C) photodetector based on vertical (Al,Ga)N/GaN nanowires grown by MBE. The current switching characteristics of the detector indicates a good repeatability. Moreover, due to the systematic analysis, the ratio of the thicknesses and the energy band difference of (Al,Ga)N and GaN sections could be the main parameters contributing to the dual-wavelength response. By using the transparent graphene, the maximum responsivity of UV-C band is over 15.5 $mA \cdot W^{-1}$, and the rejection ratio exceeds 35 times at an applied bias of -2 V. This work is pretty promising for promoting the development of dual-wavelength UV detectors for wide applications.

References

[1] Li L, Hosomi D, Miyachi Y, Hamada T, Miyoshi M and Egawa T 2017 *Appl. Phys. Lett.* **111** 102106

[2] Hao X J, Teng Y, Zhao Y, Wu Q H, Li X, Liu J F, Chen Y, Zhu H, Chen B L, Deng Z, Huang J, Huang Y and Yang H 2020 *IEEE J. Quantum Electron.* **2** 4300106

[3] Ariyawansa G, Rinzan M B M, Matsik S G, Hastings G, Perera A G U, Liu H C, Buchanan M, Sproule G I, Gavrilenko V I and Kuznetsov V P 2006 *Appl. Phys. Lett.* **89** 061112

[4] Perera A G U, Ariyawansa G, Rinzan M B M, Stevens M, Alevli M, Dietz N, Matsik S G, Asghar A, Ferguson I T, Lou H, Bezinger A and Liu H C 2007 *Infrared Phys. Technol.* **50** 142

[5] Arora K, Singh D P, Fischer P and Kumar M 2020 *Adv. Opt. Mater.* **8** 2000212

[6] Huang Z D, Weng W Y, Chang S J, Chiu C J, Hsueh T J and Wu S L 2013 *IEEE Sens. J.* **13** 3462

[7] Albrecht B, Kopta S, John O, Kirste L, Driad R, Köhler K, Walther M and Ambacher O 2013 *Jpn. J. Appl. Phys.* **52** 08JB28

[8] Liang F Z, Feng M X, Huang Y G, Sun X J, Zhan X N, Liu J X, Sun Q, Wang R X, Ge X T, Ning J Q and Yang H 2020 *Opt Express* **28** 17188

[9] Li D B, Jiang K, Sun X J and Guo C L 2018 *Adv. Opt. Photonics* **10** 43

[10] Gu Y, Yang G F, Danner A, Yan D W, Lu N Y, Zhang X M, Xie F, Wang Y K, Hua B, Ni X F, Fan Q, Gu X and Chen G Q 2020 *IEEE T. Electron Dev.* **67** 160

[11] Zhang J Y, Xing Z W, Wu D M, Bian L F, Zhao Y K, Yang W X, Wu Y Y, Zhou M, Jiang M and Shu L L 2021 *J. Cryst. Growth* **562** 126066

[12] Zhang X L, Liu B D, Liu Q Y, Yang W J, Xiong C M and Jiang X 2017 *ACS Appl. Mater. Interfaces* **9** 2669

[13] Soci C, Zhang A, Xiang B, Dayeh S A, Aplin D P R, Park J, Bao X Y, Lo Y H and Wang D 2007 *Nano Lett.* **7** 1003

[14] Jie J S, Zhang W J, Jiang Y, Meng X M, Li Y Q and Lee S T 2006 *Nano Lett.* **6** 1887

[15] Abujetas D R, Paniagua-Dominguez R and Sanchez-Gil J A 2015 *Acs Photonics* **2** 921

[16] Zhou M, Qiu H B, He T, Zhang J Y, Yang W X, Lu S L, Bian L F and Zhao Y K 2020 *Phys. Status Solidi A-Appl. Mat.* **217** 2000061

[17] Zhang X D, He T, Tang W B, Ma Y J, Wie X, Wang D H, Zhang H C, Sun H D, Fan Y M, Cai Y and Zhang B S 2020 *J. Phys. D: Appl. Phys.* **53** 495105

[18] Brems S, Verguts K, Vrancken N, Vermenulen B, Porret C, Peters L, Wu H, Huyghebaert, Schouteden K, Haesendonck C and Gendt D 2017 *ECS Transactions* **77** 3

[19] Lundquist P, Lin W P, Xu Z Y, Wong G K, Rippert E D, Helfrich J A and Ketterson J B 1994 *Appt. Phys. Lett.* **65** 1085

[20] Preschilla N A, Elkashef N M, Srinivasa R S and Major S 1998 *Surf. Coat. Technol.* **108** 328

[21] Lee J H, Hahm S H, Lee J H, Bae S B, Lee K S, Cho Y H and Lee J L 2003 *Appt. Phys. Lett.* **83** 917

[22] Nam G H, Baek S H, Cho C H and Park I K 2014 *Nanoscale* **6** 11653

[23] Wei C P, Negishi R, Ogawa Y, Akabori M, Taniyasu Y and Kobayashi Y 2019 *Jpn. J. Appl. Phys.* **58** SIIB04

[24] Ferrari A C, Meyer J C, Scardaci V, Casiraghi C, Lazzeri M, Mauri F, Piscanec S, Jiang D, Novoselov K S, Roth S and Geim A K 2006 *Phys. Rev. Lett.* **97** 187401

[25] Gao X L, Zheng L, Cheng X H, Xin W B, Ye P Y and Zhang D W 2020 *J. Mater. Sci.: Mater. Electron.* **31** 5807

[26] He T, Zhang X D, Ding X Y, Sun C, Zhao Y K, Yu Q, Ning J Q, Wang R X, Yu G H, Lu S L, Zhang K, Zhang X P and Zhang B S 2019 *Adv. Opt. Mater.* **7** 1801563

[27] Huang Y, Zhang L C, Wang J B, Chu X B, Zhang D Y, Zhao X L, Li X F, Xin L J, Zhao Y and Zhao F Z 2019 *J. Alloys Compd.* **802** 70

[28] Li Y, Li Y H, Chen J, Sun Z P, Li Z, Han X, Li P, Lin X J, Liu R Q, Ma Y W and Huang W 2018 *J. Mater. Chem. C* **6** 11666

[29] Meng R L, Ji X L, Lou Z, Yang J K, Zhang Y H, Zhang Z H, Bi W G, Wang J X and Wei T B 2019 *Opt. Lett.* **44** 2197

[30] Goswami L, Aggarwal N, Verma R, Bishnoi S, Husale S, Pandey R and Gupta G 2020 *ACS Appl. Mater. Interfaces* **12** 47038

[31] Goswami L, Aggarwal N, Singh M, Verma R, Vashishtha P, Jain S K, Tawale J, Pandey R and Gupta G 2020 *ACS Appl. Nano. Mater.* **3** 8104

[32] Jia R, Zhao D F, Gao N K and Liu D 2017 *Sci. Rep.* **7** 40483

[33] Zheng Y L, Li Y, Tang X, Wang W L and Li G Q 2020 *Adv. Optical Mater.* **8** 2000197